The Journal of Chemical Physics

Nucleation-mediated reshaping of facetted metallic nanocrystals: Breakdown of the classical free energy picture

Cite as: J. Chem. Phys. **158**, 104102 (2023); https://doi.org/10.1063/5.0138266
Submitted: 09 December 2022 • Accepted: 13 February 2023 • Accepted Manuscript Online: 14 February 2023 • Published Online: 08 March 2023

King C. Lai, Da-Jiang Liu and James W. Evans

AIP Publishing

The Journal of Chemical Physics ARTICLE scitation.org/journal/jcp

Nucleation-mediated reshaping of facetted metallic nanocrystals: Breakdown of the classical free energy picture

Cite as: J. Chem. Phys. 158, 104102 (2023); doi: 10.1063/5.0138266
Submitted: 9 December 2022 • Accepted: 13 February 2023 •
Published Online: 8 March 2023

King C. Lai,[1,2,a] Da-Jiang Liu,[1] and James W. Evans[1,2,b]

AFFILIATIONS

[1]Division of Chemical and Biological Sciences, Ames National Laboratory–USDOE, Ames, Iowa 50011, USA
[2]Department of Physics and Astronomy, Iowa State University, Ames, Iowa 50011, USA

[a]**Current address:** Fritz Haber Institut der Max Planck Gesellschaft, 14195 Berlin, Germany.
[b]**Author to whom correspondence should be addressed:** evans@ameslab.gov

ABSTRACT

Shape stability is key to avoiding degradation of performance for metallic nanocrystals synthesized with facetted non-equilibrium shapes to optimize properties for catalysis, plasmonics, and so on. Reshaping of facetted nanocrystals is controlled by the surface diffusion-mediated nucleation and growth of new outer layers of atoms. Kinetic Monte Carlo (KMC) simulation of a realistic stochastic atomistic-level model is applied to precisely track the reshaping of Pd octahedra and nanocubes. Unexpectedly, separate constrained equilibrium Monte Carlo analysis of the free energy profile during reshaping reveals a fundamental failure of the classical nucleation theory (CNT) prediction for the reshaping barrier and rate. Why? Nucleation barriers can be relatively low for these processes, so the system is not locally equilibrated before crossing the barrier, as assumed in CNT. This claim is supported by an analysis of a first-passage problem for reshaping within a master equation framework for the model that reasonably captures the behavior in KMC simulations.

I. INTRODUCTION

In the 1950s, Herring, Mullins, and others initiated analysis of the reshaping of micrometer-sized three-dimensional (3D) metallic particles mediated by surface diffusion.[1–3] Recent investigations have explored the reshaping of metallic nanoclusters[4–7] (NCs) formed via solution-phase synthesis with faceted shapes and sizes from 5 to 40 nm or 10^4–10^6 atoms.[8,9] These "larger" NCs have a bulk crystal structure. Other recent studies considered clusters with "small and intermediate" sizes below 1000 atoms, which can adopt non-bulk crystal structures, and where structural and shape evolution, as well as thermal fluxional dynamics, can occur by many-atom concerted processes.[10,11] We focus on the regime of larger NCs, where shape evolution is mediated by surface diffusion, primarily involving single-atom hops (but see Sec. II A). However, the classic Mullins-type treatment, which is based on a continuum surface diffusion equation, cannot treat reshaping for NCs with facetted synthesized shapes and equilibrium Wulff shapes. Specifically, it cannot account for the feature that evolution is controlled by the 2D nucleation and growth of new layers of atoms on outer NC facets.

These limitations of the Mullins-type treatment for reshaping of facetted 3D particles were actually recognized in the 1950s.[12,13] However, a more detailed assessment of nucleation-mediated reshaping was only provided around 2000 in an atomistic-level study by Combe *et al.*[4] for nanoscale clusters and in more coarse-grained studies by Mullins and Rohrer[14,15] based on changes in step energetics. These studies focused on the analysis of the above-mentioned 2D nucleation and growth process. As an aside, the Mullins treatment also fails for the analogous lower-dimensional problem of the reshaping of supported single-atomic-layer-thick 2D epitaxial NCs.[16–19]

In particular, for 3D NCs, Combe *et al.*[4] analyzed a generic stochastic lattice-gas model with a simple prescription of surface diffusion kinetics for the reshaping of facetted nanoclusters. A fixed initial shape distorted from the Wulff shape was assigned, so that the size of *all* facets increased with the overall NC size,

N (in atoms). Kinetic Monte Carlo (KMC) simulation analysis assessed the characteristic time for substantial shape relaxation, τ_{eq}, as a function of N for a range of temperatures, T. Observed behavior was consistent with nucleation-mediated reshaping, where one traditionally expects from classic nucleation theory (CNT) that $\tau_{eq} \sim \exp[\Delta F_{nuc}(N)/(k_B T)]$ with Boltzmann constant k_B. The nucleation barrier, $\Delta F_{nuc}(N)$, for forming new outer layers on the side facets of the NC was shown to increase with N. Additional equilibrium Monte Carlo (MC) simulations indicated an expected variation of free energy during reshaping.[14,15] No quantitative comparison was made between predictions from CNT and KMC for the reshaping barrier (see the supplementary material Sec. I). Our study will make such a comparison, but it also differs significantly in focusing on the initial stages of reshaping for only slightly truncated octahedra and nanocubes.

As indicated above, the current extensive interest in 3D metallic NCs is motivated by advances in solution-phase synthesis, which can produce facetted non-equilibrium shapes tailored to optimize performance in applications such as catalysis or plasmonics.[8,9] Thus, the shape stability of such NCs is key to avoiding degradation of performance. Considering structure-sensitive catalytic reactions, it is natural to utilize octahedra and nanocubes for reactions optimized on fcc {111} and fcc {100} facets, respectively. This study will analyze the reshaping of: (i) Pd octahedra synthesized with minority {100} facets at the truncated corners or vertices,[20,21] which are used for catalysis,[22,23] and H-storage;[24,25] (ii) Pd nanocubes synthesized with minority {111} facets at the corners, and minority {110} facets along the edges[16,26] also used for catalysis.[16,27–29] Octahedra[30–32] and nanocubes[33–35] have also been synthesized for multiple other metals. Recent studies comparing reshaping rates of nanocubes and octahedra have suggested a correlation with barriers for single-atom terrace diffusion across {100} vs {111} facets,[36] or for extraction from edges to side facets.[37] However, as indicated above, reshaping is a cooperative many-body process, and appropriate nucleation theoretic concepts should be invoked, although we shall reveal a fundamental failure of CNT to provide a quantitative description of reshaping.

Indeed, our focus in this contribution is on providing a critical assessment of the applicability of the CNT picture for the reshaping of facetted fcc metallic NCs of at least 5 nm or $\sim 10^4$ atoms, sizes typical for solution-phase synthesis. A detailed analysis is provided for the reshaping of slightly truncated fcc metal octahedra and nanocubes utilizing a model crafted to realistically describe the kinetics of surface diffusion for fcc metals. Parameters are chosen to correspond to Pd, but the basic conclusions apply for any fcc metal. We extend previous KMC studies yielding precise results for the effective barrier for reshaping, thereby providing benchmark results for subsequent analysis. Then, we perform constrained equilibrium MC simulations to determine free energy profiles during reshaping for our model and associated free energy barriers. We find a substantial discrepancy between effective barrier predictions from this conventional CNT-type free energy profile analysis and those from the KMC simulation. We elucidate the discrepancy between the CNT predictions and the actual kinetics by a novel formulation of reshaping as a first-passage problem within a master equation (MEQ) framework. The latter provides a fundamental description of evolution in stochastic models.

II. MODELING AND SIMULATION METHODS

A. Stochastic lattice-gas modeling

We adopt a previously developed[38] stochastic lattice-gas model for NC evolution with atoms at fcc lattice sites subject to an effective nearest-neighbor (NN) attractive interaction of strength $\phi_{eff} > 0$. The successful use of effective NN interactions for description of surface thermodynamics and diffusion processes for fcc metals has been confirmed by density functional theory (DFT) analysis.[39] Under-coordinated surface atoms hop to empty NN fcc surface sites with Arrhenius rates, $h = \nu \exp[-E_{act}/(k_B T)]$, where E_{act} is a local environment-dependent activation barrier, and ν a common prefactor. In the following, n_{init} (n_{fnl}) denote the initial (final) coordination of an atom before (after) hopping, and $E_{init} = -n_{init}\,\phi_{eff}$ ($E_{fnl} = -n_{fnl}\,\phi_{eff}$) are the corresponding energies.

Most previous lattice-gas studies of NC evolution have employed a generic bond-breaking prescription, $E_{act} = E_0 - E_{init}$, also known as an initial value approximation (IVA), where E_0 is an adjustable parameter.[4–7] However, other prescription of barriers has also been employed, including a recently developed prescription that effectively allows adjustment of the location of the transition state relative to initial and final states.[40,41] This capability is in the spirit of the Bronsted-Evans-Polyani (BEP) formulation, a symmetric version of which is a common choice for treatment of surface diffusion.[42] All these choices, as well as a Metropolis prescription, satisfy the essential constraint of detailed-balance that ensures that evolution will lead to the correct thermodynamic equilibrium state. However, the IVA prescription, as well as all these other generic formulations, fails to capture even some of the basic features of diffusion on fcc metal surfaces, such as the relative values of barriers for terrace diffusion of different facets or for step edge vs terrace diffusion, or the presence of Ehrlich–Schwoebel barriers.[7,43] Trends in and reliable values for barriers are well-established through extensive studies by the experimental and theoretical surface science community focusing on the growth and post-deposition evolution of homoepitaxial metal films.[7,43–46]

Realistic treatments of surface diffusion kinetics in modeling are rare.[7,38,47,48] Our approach to avoid the shortcomings of generic treatments is to adopt a refinement of a symmetric BEP formulation, $E_{act} = E_\alpha + 1/2\,(E_{fnl} - E_{init})$. Contrasting traditional BEP implementation for surface diffusion,[42] all possible hops of surface atoms are divided into several classes, α, for terrace diffusion on {100} and {111} facets, for edge diffusion along {100}- and {111}-microfacetted steps, etc., while still satisfying detailed-balance. This refinement provides the flexibility for E_{act} to recover precise DFT values for multiple key barriers in these classes by appropriate selection of E_α.[7,38,48]

Based on our DFT analysis for Pd,[48,49] for terrace diffusion, we choose $E_\alpha = 0.11$ eV on {111} facets and $E_\alpha = 0.65$ eV on {100} facets. For diffusion along straight steps, we choose $E_\alpha = 0.45$ eV for along {100}-microfacetted steps and $E_\alpha = 0.42$ eV along {111}-microfacetted steps. We also choose $\delta_{ES} = 0.22$ eV for the additional Ehrlich–Schwoebel step edge barrier. Finally, we select $\phi_{eff} = 0.32$ eV for Pd optimally recovers surface thermodynamics. In contrast, to recover bulk thermodynamics for Pd, one would choose an NN-interaction $\phi_{bulk} = E_{coh}/6 = 0.65$ eV, where $E_{coh} = 3.89$ eV is the bulk cohesive energy for Pd.

On some fcc metal surfaces, two-atom concerted exchange diffusion processes for terrace and interlayer diffusion have lower barriers than single-atom hopping. However, this feature can be effectively captured by the above type of modeling with single-atom hopping by selecting E_α to match the barrier for any more facile concerted process, as demonstrated by previous successful modeling of thin film growth.[43]

B. Initial truncated nanocluster geometries

Experimental synthesis cannot produce perfect complete nanocubes or octahedra but rather these have various degrees of truncation at the corners and/or edges, as noted in Sec. I. For convenience, we consider one-parameter families of initial truncated geometries of octahedra and nanocubes. For *octahedra*, we consider various degrees of truncation of the six vertices of a complete octahedron to produce {100} corner facets of different sizes. Truncations with (j + 1) × (j + 1) atom {100} facets at the vertices for j ≥ 1 are denoted by TRj [see Fig. 1 (top)]. For these octahedra, we do not truncate the edges since the central edge atoms have a high coordination of 7. For *nanocubes*, the jth-order truncation, TRj, creates {110} edge facets with a width corresponding to rows of length L_e = j + 1 atoms. Edge truncation automatically exposes generally distorted hexagonal {111} corner facets with three edges of length L_e, but the other three having length $L_c \geq L_e$. For each L_e, we choose an appropriate value of L_c, thereby obtaining a one-parameter family, TRj[48] [see Fig. 1 (bottom) and supplementary material Sec. III]. Reshaping will primarily involve the transfer of atoms from narrow edge facets for nanocubes, or small vertex (or corner) facets for octahedra, to form new layers on the large side facets.

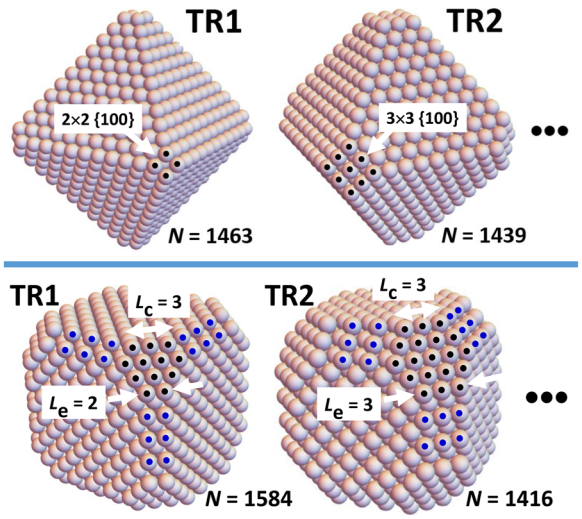

FIG. 1. Schematics of NC truncations TR1 and TR2 (for small NC sizes to highlight atomistic details). Top: octahedra with surface atoms in a corner {100} facet indicated by black dots. Bottom: nanocubes with surface atoms in a corner {111} facet indicated by black dots, and edge atoms in {110} facets close to this corner facet indicated by blue dots.

C. KMC and MC simulation, and MEQ analysis

KMC simulations to precisely track kinetics of the stochastic atomistic-level model for reshaping implement atomistic hopping processes with probabilities proportional to their physical rates. A rejection-free simulation algorithm is implemented to enhance computational efficiency given the broad distribution of possible hop rates. As evolution tracked by KMC is stochastic, many KMC trials are typically run to accurately capture average behavior. In the majority of cases, we run 200 trials for smaller NCs with N ~ 10^4. However, in some cases, for larger NC sizes and/or lower T, less trials are run as the simulation is computationally more expensive. A comprehensive listing of the number of trials for different cases is provided in the supplementary material Sec. II. The key point is that we run a sufficient number of trials so that our KMC results are quantitatively accurate.

Equilibrium Monte Carlo simulations are employed to obtain the system free energy, $F(q)$, as a function of the number, q, of atoms transferred from edges or vertices to side facets. These probe equilibrium configurations in our NC model within a constrained window, $q- \leq q \leq q+$, by blocking events that would lead to a q-value outside this range.[50] For computational efficiency, simulations are often performed for multiple contiguous smaller widows rather than a single large window covering the q-range of interest. Then, results for the probability, $P(q)$ for q transferred atoms are pieced together to generate a continuous $P(q)$ and thus $F(q)$, as presented in Sec. III B.

For viable master equation (MEQ) analysis, it is essential to judiciously select a subset of key NC configurations for the reshaping process. Key input to the MEQ analysis is the energetics and degeneracies of these configurations, as well as the rates for transitions between them. Quantitative analysis of the master equations is performed by numerical integration.

III. KMC AND MC ANALYSIS OF RESHAPING FOR OCTAHEDRA AND NANOCUBES

As noted above, solution-phase synthesis of octahedra and nanocubes produces geometries with some degree of truncation of corners and/or edges. Reshaping primarily involves transfer of atoms from the small corner and/or narrow edge facets to the much larger side facets. This leads to nucleation and growth of 2D islands (i.e., formation of new outer layers) of atoms on those side facets.

A. KMC simulation results for reshaping

KMC simulations of reshaping start with configurations corresponding to the truncations TRj and track evolution for the above stochastic model. Figure 2 illustrates the evolution for small NCs with truncation TR1. However, our quantitative analysis (which focuses on much larger sizes) tracks evolution until the formation of the first 2D island on a side facet reaching the prescribed critical size, q_c (in atoms), and identifies that time, τ_{eq}, as the characteristic time for the initial stages of shape relaxation. For lower-order truncations, j = 1–3, we select q_c = 19 for octahedra (for a hexagonal island on a {111} facet with side length three atoms), and q_c = 9 for nanocubes (for a square island on a {100} facet with side length three atoms). That these are reasonable choices for critical sizes is indicated by the free energy analysis in Sec. III B, and also by previous analytic studies.[48,51] Thus, one expects that by replacing q_c

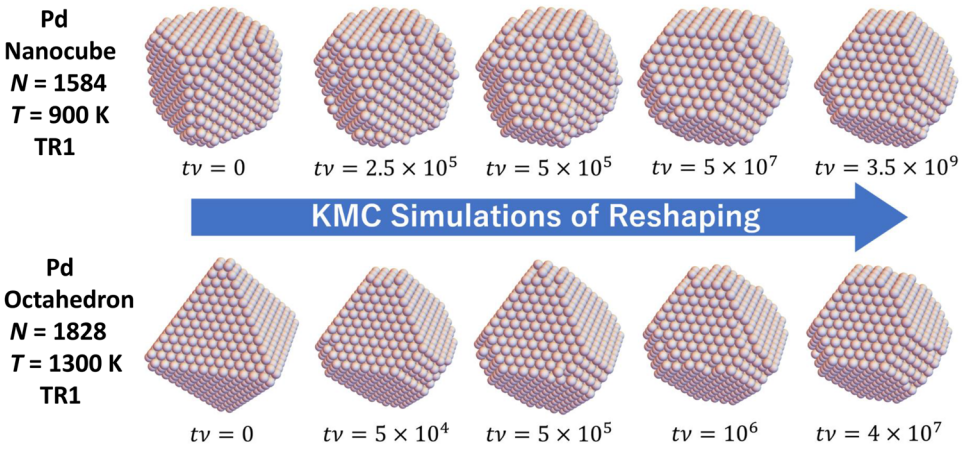

FIG. 2. KMC simulation illustrating reshaping of a Pd nanocube (octahedron) of size $N = 1584$ ($N = 1828$) atoms at 900 K (1300 K) with initial truncation TR1. We show images for small sizes to highlight the atomistic details of configurations, but our analysis will focus on larger sizes.

TABLE I. KMC simulation results for the effective barrier, $E_{eff} = E_{eff}$(KMC), for reshaping of truncated Pd nanocubes (cube) and octahedra (oct).

Cube E_{eff} for TR1 (600–800 K)	1.30 eV @ $N = 7649$	1.27 eV @ $N = 34\,201$
Cube E_{eff} for TR2 (750–900 K)	1.87 eV @ $N = 7209$	1.90 eV @ $N = 33\,569$
Cube E_{eff} for TR3 (900–1150 K)	2.24 eV @ N = 7730	2.27 eV @ $N = 31\,845$
Oct E_{eff} for TR1 (1000–1300 K)	1.08 eV @ $N = 8113$	0.93 eV @ $N = 33\,775$
Oct E_{eff} for TR2 (1100–1400 K)	2.27 eV @ $N = 8089$	2.02 eV @ $N = 33\,751$
Oct E_{eff} for TR3 (1200–1500 K)	2.84 eV @ $N = 8035$	2.56 eV @ $N = 33\,697$

with a larger value will make little difference to τ_{eq}, as a 2D island that reaches the critical size will quickly grow thereafter. Results for τ_{eq} relevant for our subsequent analysis are summarized in Table I (see also supplementary material Sec. IV). Arrhenius analysis of $\tau_{eq} \sim \exp[E_{eff}/(k_B T)]$ has shown previously that the effective barrier, E_{eff}, increases strongly with an order of truncation.[48,51] Here, we emphasize the feature that E_{eff} for nanocubes depends extremely weakly on the overall NC size, N, for a specific truncation. Octahedra exhibit only a slightly stronger systematic decrease in E_{eff} with increasing N. This behavior is in marked contrast to the strong dependence of E_{eff} on N for reshaping, where all NC facets have comparable size.[4] In addition, we note that while a single value can reasonably be assigned for E_{eff} over a narrower T-range of width $\Delta T \approx 200$–300 K, our analysis over a broader T-range (presented later) indicates that E_{eff} systematically decreases with increasing T.

B. Free energy variation from constrained equilibrium MC sampling

One might attempt to obtain additional insight into NC reshaping from an assessment of the variation of the free energy, $F(q)$, vs the number of transferred atoms, q, from NC corners and/or edges to side facets during reshaping.[4] Then, the CNT-based free energy barrier, ΔF_{nuc}, and the associated effective barrier for reshaping, E_{eff}(CNT), satisfy

$$\Delta F_{nuc} = \max_q [F(q) - F(0)], \text{ and } E_{eff}(\text{CNT}) = \Delta F_{nuc} + E_{diff}, \quad (1)$$

where E_{diff} is an appropriate activation barrier for surface diffusion, as described in the following. In this formulation, for each q, the system is assumed to be in a constrained equilibrium (at least for q below a critical size). However, such local equilibration requires a separation of time scales in the actual stochastic model between slow processes leading to evolution along the "reshaping reaction pathway" for increasing q and fast processes "orthogonal" to that pathway.

To obtain $F(q)$, we implement equilibrium Monte Carlo simulations utilizing an umbrella sampling type approach.[45] Simulations probe equilibrium configurations in our NC reshaping model within a constrained window, $q- \le q \le q+$, where q is the number of atoms transferred to side facets. One extracts the probability, $P(q)$, for $q- \le q \le q+$ for the constrained system to be in a configuration with exactly q transferred atoms. Then, the free energy follows from $F(q) = -(k_B T) \ln[P(q)]$ to within an arbitrary reference. We expect that near the peak of $F(q)$ vs q, transferred atoms are typically arranged into a single 2D island on a single side facet. Since $F(q)$ should primarily reflect NC configurations with surface atoms incorporated into 2D islands or complete facets, we argue that $E_{diff} = E_d + E_{ex}$ should include the energy cost, E_{ex}, of atom extraction from the island as well as an appropriate terrace diffusion barrier, E_d. For octahedra, we select $E_d \approx 0.1$ eV as the Pd diffusion barrier on {111} facets, and for nanocubes $E_d \approx 0.65$ eV as the Pd diffusion barrier on {100} facets. We also select $E_{ex} \approx 3\phi_{eff} \approx 0.9$ eV for octahedra, and $E_{ex} \approx 2\phi_{eff} \approx 0.6$ eV for nanocubes, reflecting typical extraction energies.

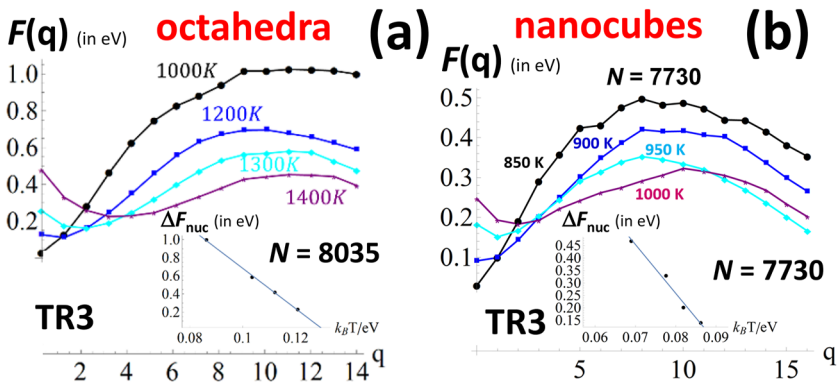

FIG. 3. Equilibrium MC simulation of the free energy profiles (left) $F(q) = -(k_B T)\ln[P(q)]$ vs the number of transferred atoms, q. (a) Reshaping of TR3 Pd octahedra with $N = 8035$, where atoms are transferred to {111} facets. (b) Reshaping of Pd nanocubes with $N = 7730$, where atoms are transferred to {100} facets. Insets: free energy barrier, ΔF_{nuc}, vs $k_B T$.

Figure 3 shows results for $F(q)$ vs q from such an analysis for Pd octahedra and nanocubes with size $N \approx 0.8 \times 10^4$ for truncation TR3 and for a range of T. $\Delta F_{nuc} = \Delta F_{nuc}(T)$ decreases strongly with increasing T (see insets). We emphasize that results for ΔF_{nuc} and the corresponding E_{eff}(CNT) are *not* consistent with E_{eff}(KMC) for the same range of higher T. For TR3 octahedra, KMC analysis for reshaping from 1200 to 1500 K yielded E_{eff}(KMC) $\approx$ 2.8 eV. However, E_{eff}(CNT) $\approx$ 1.6 eV at 1200 K is far lower. For TR3 nanocubes, KMC analysis for reshaping from 900 to 1150 K yielded E_{eff}(KMC) $\approx$ 2.2 eV. However, E_{eff}(CNT) $\approx$ 1.5 eV at 900 K is again far lower. Figure 3 shows results for only one truncation and one NC size. However, extensive additional results reported in the supplementary material Sec. V for octahedra for truncations TR2–TR4, and supplementary material Sec. VI for nanocubes for TR3, and sizes from $N \approx 0.8 \times 10^4$ to $N \approx 3 \times 10^4$, all display similar behavior. In particular, these results show a systematic increase in ΔF_{nuc} with truncation order for a fixed T. Furthermore, they show that $F(q)$ varies only weakly with N, consistent with our view that reshaping should not depend strongly on NC size. Finally, for a discussion of the initial decrease of $F(q)$ with q at higher T, see supplementary material Sec. VII.

IV. MASTER EQUATION ANALYSIS vs CNT AND KMC

A. Overview

Using constrained equilibrium sampling to determine free energy profiles is effective in elucidating kinetic phenomena such as classical nucleation with large barriers where the system is close to locally equilibrated before crossing the barrier. However, we hypothesize that the "low barrier" reshaping processes considered here do not achieve such local equilibrium. In that case, equilibrium simulations sample more states for each number q of transferred atoms than sampled in kinetic evolution. Then, the associated entropic contribution assuming local equilibration would lower the barrier for reshaping more significantly that in the kinetic simulations.

The above hypothesis motivates the development of a theoretical treatment of NC reshaping kinetics without any *a priori* assumption of local equilibration for each q. Such a treatment can, in principle, be formulated as a first-passage time problem utilizing the master equations (MEQ) for the stochastic model.[52] Specifically, these equations track the evolution of the probabilities for the NC to be in various configurations or states starting from a prescribed initial state, TRj with $q = 0$. States for $q > 0$ are progressively populated with increasing time. Such states include those on the optimal or minimal energy path (MEP) for reshaping, which involves configurations with the lowest energy $E(q)$ for each q. We can exactly determine the energy change $\Delta E(q) = E(q) - E(0)$, and furthermore emphasizes that $\Delta E_{max} = \max_q \Delta E(q)$ is a key parameter in determining reshaping kinetics. In this respect, we note that the free energy barriers for nucleation $\Delta F_{nuc}(T)$ assessed in Sec. III B satisfy $\Delta E_{max} = \Delta F_{nuc}(T \to 0)$ (see supplementary material Sec. IV). Naturally, stochastic evolution during reshaping leads to a population of states not just along the MEP, but also "orthogonal" to this pathway (i.e., states with higher energy for each q). Once a sufficiently large 2D island of say $q = q^*$ atoms has formed on a side facet, where q^* exceeds some critical size, q_c, and the energy on the MEP has decreased well below its maximum, then the likelihood of the system evolving back toward the initial state is negligible. Thus, one can regard $q = q^*$ as being a trapping or absorbing state in the evolution upon blocking transitions with $q > q^*$, and then analyze the master equations with this trapping boundary condition.

Specifically, one can determine the probability, $P_{q=q^*}(t)$ for the system to be in the trapping state with $q = q^*$, where this quantity increases monotonically in time from 0 to 1. One can then extract a characteristic time for shape relaxation, τ_{eq}, from the time when $P_{q=q^*}(t)$ reaches some assigned threshold value, e.g., $P_{q=q^*}(\tau_{eq}) = 1/2$. Performing such an analysis for a narrow range of temperature around a target temperature, T, yields an effective barrier $E_{eff} = E_{eff}$(MEQ) for reshaping, which will depend on the target T. Results can be compared with those from KMC, or from the free energy analysis.

Our master equation treatment will necessarily include various approximations. A major challenge is that evolution occurs in a multi-dimensional space involving a vast number of NC configurations. A viable treatment requires identifying and explicitly treating only a subset of states that are most significant. Also, our master equation formalism will not include transitions between individual states connected by single-atom hops, as in the KMC simulation of the stochastic model. Rather, all states with one isolated adatom on a side facet will be grouped into a single state. Nonetheless, this treatment should capture the key features of behavior in the reshaping process.

B. Master equation analysis for TR1 octahedra: Detailed example

1. Selection of states for the MEQ analysis

We first describe the master equation formulation for octahedra with truncation TR1, where Fig. 4 illustrates a subset of significant states explicitly included in the analysis, together with the allowed transitions between them. States on the lowest row in Fig. 4 correspond to the lower component of the MEP where q atoms are transferred from consecutive 2×2 {100} corner facets to form a single 2D island on a {111} side facet, so as to minimize the relative energy, $\Delta E(q) = E(q) - E(0)$, for each $q = 0, 1, \ldots$. However, evolution between these states for consecutive q necessarily occurs by transitions through states on the second lowest row in Fig. 4, which can be regarded as the upper component of the MEP. These states, which include one isolated adatom on a {111} facet transferred from a {100} facet and which has yet to join an island of n atoms on a {111} facet, are labeled by n ⊕ 1. Energies changes, ΔE, are listed for both components of the MEP in Table II, revealing a maximum $\Delta E_{max} = 6\phi_{eff}$ on the upper component of the MEP (see also supplementary material Sec. VIII).

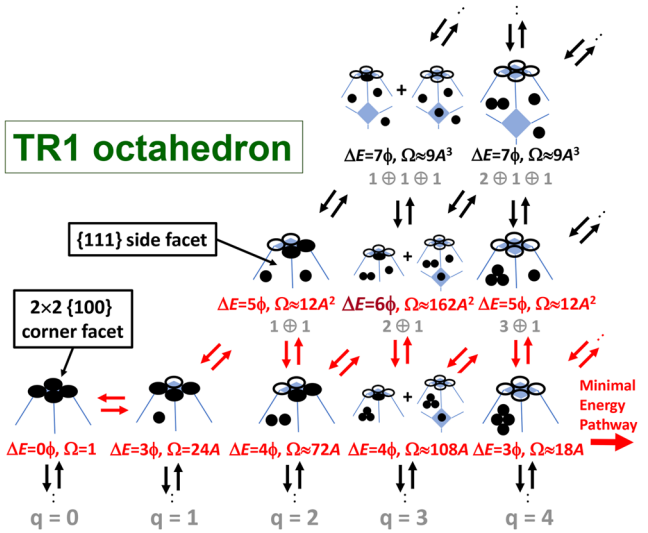

FIG. 4. Key NC states for a TR1 octahedron and transitions between them in our master equation treatment. ΔE (writing ϕ for ϕ_{eff}) are state energies, and Ω are degeneracies (see supplementary material Sec. VIII). A is the total area (in adsorption sites) for all {111} side facets. Open circles indicate locations on {100} corner facets from which atoms (solid circles) were transferred to {111} side facets. Red arrows indicate transitions along the MEP.

Our formulation also includes other selected states off the MEP with the highest degeneracies, the analysis of which is described in more detail in supplementary material Sec. IX. These states would have significant population relative to the MEP states as determined by the Gibbs distribution if the system is locally equilibrated. In these states, the single 2D island in the MEP state has been fragmented, and the multiple atoms and smaller clusters can populate different or the same {111} side facet. Figure 4 illustrates the former. This fragmentation results in high state degeneracies due to the large total area, A (measured in adsorption sites), of the {111} side facets and thus a large number of possible locations of the 2D island and/or of the isolated adatoms on {111} side facets.

We assign the MEP state with $q = q^* = 12$, where $\Delta E(q^*) = 0$ as the trapping state. Then, in our master equation analysis, the system can evolve into but not out of this state, so transitions to states with $q \geq 13$ are blocked. A total of 79 distinct states are retained in this master equation analysis with $q^* = 12$.

Regarding approximations in our MEQ treatment, we only include explicitly a small portion of states off the MEP with the highest configurational degeneracy. Arrows at the bottom of Fig. 4 indicate possible transitions to other states. For example, just for $q = 0$, atoms can be transferred between {100} facets, or from the edges separating {111} facets to {100} facets. Analogous states exist for each $q > 0$. The degeneracy of these states is relatively small being controlled by the number of vertices and the length of edges rather than the area of {111} facets. Also, as noted above, we group many individual states into a single state (e.g., states with different locations of one isolated atom on a side facet are grouped into a single state denoted n ⊕ 1). This may induce a higher degree of local equilibration than in the stochastic model (cf. Sec. IV B 2).

The rates for "forward" transitions in the master equations have the form $k = \nu\, m \exp[-(n\phi_{eff} + E_d)/(k_B T)]$, where ν is a prefactor, and E_d is the terrace diffusion barrier for {111} facets. For upward diagonal transitions in Fig. 4 with increasing q, one has $n = n_{100} - n_{111}$ where $n_{100} = 6$, 5, or 4 is the initial coordination of the atom which is moved from the {100} facet, and $n_{111} = 3$ is its coordination as an isolated adatom on the {111} facet (before joining the growing 2D island). Thus, n corresponds to the magnitude of the reduction in coordination moving from the {100} to {111} facet. In this prescription, atoms with the minimum n are selected, and m denotes the number of such atoms on {100} facets. For upward vertical transitions involving detaching atoms from the 2D island onto the {111} facet, n denotes the number of lateral bonds broken upon detachment from the island. Again, atoms with the minimum n are selected, and m denotes the number of such atoms. Thus, in both cases, $n\phi_{eff} + E_d$ corresponds to an "extraction barrier." Rates for "reverse" transitions follow from those for forward transitions via the detailed-balance constraint and thus depend on the

TABLE II. Energies for states along the MEP for the TR1 octahedron both for the lowest row in Fig. 4 (states q = n) and the second lowest row (states n ⊕ 1). Bold: states with $\Delta E = \Delta E_{max}$.

n	0	1	2	3	4	5	6	7	8	9	10	11	12
$\Delta E(q = n)/\phi_{eff}$	0	3	4	4	3	4	4	3	2	3	2	2	0
$\Delta E(n \oplus 1)/\phi_{eff}$		5	**6**	5	**6**	**6**	**6**	4	5	5	4	3	3

energies and degeneracies of initial and final states shown in Fig. 4 (see supplementary material Sec. X for examples and supplementary material Sec. XI for a complete listing of energetics and forward rates along the MEP).

2. MEQ results and comparison with other treatments

In the following, we compare results for $E_{eff} = E_{eff}(MEQ)$ from a master equation analysis with $E_{eff}(KMC)$ from KMC simulation, as well as with $E_{eff}(CNT)$ from an analytic version of a CNT-type free energy analysis. For the latter, we note that the free energy for a set of states, S, relative to that of the non-degenerate initial state $q = 0$ can be calculated from

$$\Delta F(S) = -(k_B T)\ln[\,Q(S)],$$

where

$$Q(S) = \sum_j \Omega j(S)\exp[-\Delta E_j(S)/(k_B T)], \quad (2)$$

where $\Omega_j(S)$ and $\Delta E_j(S)$ are the degeneracies and relative energies of the states in S labeled by j, respectively. The free energy barrier ΔF_{nuc} is obtained by choosing $S = S_{TS}$ as the transition state, and then $E_{eff}(CNT) = \Delta F_{nuc} + E_{diff}$, where E_{diff} is an appropriate surface diffusion barrier. In this analysis, since ΔF_{nuc} will be determined from a transition state S_{TS} corresponding to a 2 ⊕ 1 type state that already has an isolated adatom, E_{diff} just corresponds to an appropriate terrace diffusion barrier $E_d = 0.11$ eV for diffusion on {111} facets (i.e., it does not include an additional extraction energy contribution as in Sec. III B). With $S_{TS} = 2 \oplus 1$ for TR1 octahedra, one has that

$$\Delta F_{nuc} \approx \Delta E_{max} - (k_B T)\ln(162A^2) = 6\Phi_{eff} - (k_B T)\ln(162A^2). \quad (3)$$

Choosing $S_{ST} = \{2 \oplus 1, 1 \oplus 1 \oplus 1\}$ just gives a somewhat lower value of ΔF_{nuc}. Note that other MEP states (4 ⊕ 1, etc.) with $\Delta E = \Delta E_{max} = 6\phi_{eff}$ correspond to a lower ΔF due to higher degeneracy and thus do not determine ΔF_{nuc}.

Figure 5 and Table III show results for E_{eff} vs T for $N = 8113$ (corresponding to $A \approx 2000$) from (i) more extensive KMC simulations, which in contrast to those reported in Table I allow assessment of the T-dependence of E_{eff} (see also supplementary material Sec. XII); (ii) our master equation analysis using $P_{q=q^*=12}(\tau_{eq}) = 1/2$ (where P_{12} is the probability to be in any state with 12 transferred atoms), with $E_d = 0.11$ eV; and (iii) our analytic free energy analysis with $S_{TS} = 2 \oplus 1$ with $E_d = 0.11$ eV. A key feature emerging from these analyses is that E_{eff} exhibits a systematic decrease with increasing T. $E_{eff}(MEQ)$ and $E_{eff}(KMC)$ are both far above $E_{eff}(CNT)$, consistent with our proposal that the NC is not locally equilibrated for each q during reshaping. There is reasonable consistency between KMC and MEQ predictions, certainly regarding the variation with T. However, a systematic discrepancy is also evident with $E_{eff}(KMC)$ slightly exceeding $E_{eff}(MEQ)$. This discrepancy is explained in terms of the above-mentioned feature of our MEQ treatment, specifically grouping into a single state n ⊕ 1 many individual states with different locations of one isolated atom on a side facet. This feature is anticipated to induce a higher degree of local equilibration among configurations with a fixed number of transferred atoms than in the stochastic model. This, in turn, results in a slight artificial lowering of E_{eff} (analogous to the same stronger effect in the CNT treatment).

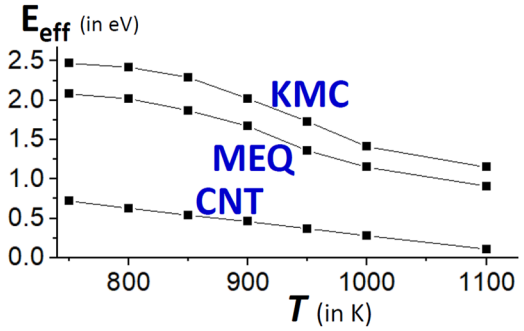

FIG. 5. E_{eff} vs T for reshaping of TR1 truncated Pd octahedra with $N = 8113$. Comparison of results from KMC simulation (KMC), master equation analysis (MEQ), and a free energy analysis (CNT) with $S_{TS} = 2 \oplus 1$, setting $E_d = 0.11$ eV.

TABLE III. E_{eff} (in eV) vs T for reshaping of TR1 truncated Pd octahedra with $N = 8113$ from KMC simulation (KMC), master equation analysis (MEQ), and a free energy analysis (CNT).

TR1 octahedron	750 K	800 K	850 K	900 K	950 K	1000 K	1100 K
E_{eff}(KMC)	2.47	2.42	2.29	2.02	1.73	1.41	1.15
E_{eff}(MEQ)	2.08	2.02	1.87	1.67	1.36	1.15	0.91
E_{eff}(CNT)	0.72	0.63	0.54	0.46	0.37	0.28	0.11

Finally, we note that a further simplified master equation analysis retaining a more restricted set of states, specifically just those along the MEP, yields qualitatively similar E_{eff} to $E_{eff}(MEQ)$ reported here from the more complete master equation analysis (except for higher T above 1000 K) (see supplementary material Sec. X).

C. Master equation analysis for other TRj octahedra and nanocubes

1. TRj octahedra with j > 1

From the analysis of energy changes, ΔE, for states along the MEP, one finds that $\Delta E_{max} = 9\phi_{eff}$ for TR2, $\Delta E_{max} = 11\phi_{eff}$ for TR3, and so on (vs $\Delta E_{max} = 6\phi_{eff}$ for TR1). The rates for forward transitions in the master equations have the same form as for TR1, and those for reverse transitions are again determined by detailed-balance. We have implemented a master equation (MEQ) analysis, but just for TR2 with $N = 8089$ where the total area of {111} side facets is $A \approx 1980$, and just retaining states along the MEP. One could assign $q^* = 27$ where $\Delta E(q^*) = 0$ as the trapping state. However, to reduce the number of retained equations in the MEQ treatment, we will choose $q^* = 18$ where $\Delta E(q^*) = 3\phi$ is already well below ΔE_{max} (see supplementary material Sec. X for a listing of the energies and degeneracies of all states, as well as transition rates between them). The general conclusion is the same as for TR1. $E_{eff}(MEQ)$ for TR2 Pd octahedra are significantly above $E_{eff}(CNT) = \Delta F_{nuc} + E_d$ assigning $S_{TS} = 6 \oplus 1$ with degeneracy $\Omega \approx 2688A^2$ as the transition state, and setting $E_d = 0.11$ eV as for TR1 octahedra (see Table IV). For the TR2 case, one has that $E_{eff}(KMC) \approx 2.2$ eV at 1100–1400 K roughly compatible with $E_{eff}(MEQ)$ at around 1100 K, and more detailed analysis of the limited KMC data indicates that $E_{eff}(KMC)$ does decrease with increasing T.

TABLE IV. E_{eff} (in eV) for reshaping of TR2 truncated Pd octahedra with $N = 8089$ from a master equation analysis just including MEP states, $(MEQ)|_{MEP}$, and from a free energy analysis (CNT) with $S_{TS} = 6 \oplus 1$, and setting $E_d = 0.11$ eV. Note that $E_{eff}(KMC) \approx 2.2$ eV at 1100–1400 K.

TR2 octahedra	850 K	950 K	1050 K	1150 K	1250 K
$E_{eff}(MEQ)\|_{MEP}$	2.87	2.63	2.19	1.72	1.38
$E_{eff}(CNT)$	1.30	1.10	0.90	0.70	0.63

TABLE V. E_{eff} (in eV) for reshaping of TR1 truncated Pd nanocubes with $N = 1584$ from a master equation analysis just including MEP states, $(MEQ)|_{MEP}$, and from a free energy analysis (CNT), and setting $E_d = 0.65$ eV. Note that $E_{eff}(KMC) \approx 1.3$ eV at 600–800 K.

TR1 nanocubes	450 K	550 K	650 K	750 K	850 K
$E_{eff}(MEQ)\|_{MEP}$	1.71	1.36	1.18	1.09	1.02
$E_{eff}(CNT)$	1.10	0.92	0.73	0.56	0.37

2. TRj nanocubes for $j \geq 1$

In this case, atoms tend to be transferred from {110} edges to {100} side facets of nanocubes, so the total length, L, of edges (measured in atoms), as well as the total area, A, of side facets (measured in adsorption sites), feature in the state degeneracies. For TR1 nanocubes, Fig. 6 shows a subset of particularly significant states and the transitions between them, analogous to Fig. 4 for TR1 nanocubes. Analysis of the MEP reveals that $\Delta E_{max} = 4\phi_{eff}$ (see Sec. IV C 3 and supplementary material Sec. XIII). For this system, one might reasonably select $q^* = 16$ where $\Delta E(q^*) = 0$ as the trapping state. We have implemented a master equation analysis, but just for TR1 and just retaining states along the MEP. The rates for forward transitions in the master equations have the same form as for nanocubes (except that now $n = n_{110} - n_{100}$ with $n_{110} = 5$ or 6 and $n_{100} = 4$), and those for reverse transitions are again determined by detailed-balance (see supplementary material Sec. XII for further details). Results are presented in Table V selecting a smaller NC with $N \approx 1584$ where $A \approx 360$ and $L \approx 60$, which reduces degeneracies and thus reduces the influence of neglected states not on the MEP. We also show results for $E_{eff}(CNT) = \Delta F_{nuc} + E_d$ assigning the state

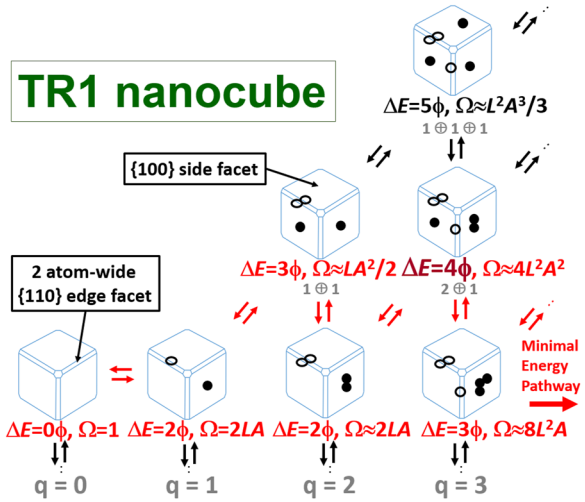

FIG. 6. Key states and allowed transitions between them for a TR1 nanocube in our master equation treatment. ΔE (writing ϕ for ϕ_{eff}) are state energies and are Ω degeneracies (see supplementary material Sec. XII). A is the total area (in adsorption sites) for all {100} side facets, and L the total edge length (in atoms) of all {110} edges. Open circles indicate locations from which edge atoms (solid circles) were transferred to {100} side facets. Red arrows: transitions along the MEP.

$S_{TS} = 2 \oplus 1$ with degeneracy $\Omega \approx 4L^2A^2$ as the transition state. Here, $E_d \approx 0.65$ eV is the diffusion barrier for Pd on a {100} facet. $E_{eff}(MEQ)$ values are more consistent with $E_{eff}(KMC) \approx 1.3$ eV at 600–800 K than the much lower $E_{eff}(CNT)$.

Master equation analysis for nanocubes can be extended to higher-order truncations, where $\Delta E_{max} = 6\phi_{eff}$ for TR2, $\Delta E_{max} = 7\phi_{eff}$ for TR3 (vs $\Delta E_{max} = 6\phi_{eff}$ for TR1). See Sec. IV C 3 and supplementary material Sec. XIV. As for octahedra, a significantly higher number of states and equations must be retained for these higher-order truncations. Also, again $E_{eff}(CNT)$ is well below reliable estimates of E_{eff}.

3. Dependence of reshaping on truncation order

From the KMC results reported in Table I, it is clear that for both octahedra and nanocubes, the effective barrier, E_{eff}, for reshaping systematically increases with truncation order. This same trend is captured in our MEQ analysis (e.g., compare results in Tables III and IV for TR1 and TR2 octahedra, respectively, consistently choosing the same T). Furthermore, even though the CNT treatment greatly underestimates E_{eff} values, it does also incorporate this trend.

This trend might seem surprising as higher-order truncated structures might seem to be intermediate structures in the evolution of lower-order truncated structures toward equilibrium Wulff shapes. In particular, during reshaping toward a Wulff shape, one might expect that a TR1 NC would evolve through an intermediate TR2 (or TR3, etc.) structure as outer layers of atoms are removed from the small edge or corner facets. This would imply that TR1 reshaping would be controlled by the higher effective barriers for TR2, TR3, etc. structures. However, these intermediate structures for TR1 NCs are not perfect TR2, TR3, etc. structures as the atoms removed from edge or corner facets have formed a 2D island on a large side facet. The presence of this 2D island substantially reduces the cost of removing further atoms from the intermediate structure (relative to a perfect TR2, TR3, etc. structure). Also, at this stage in evolution, the system energy is well below the initial energy (i.e., the system is well past the "transition state").

We also emphasize that our analysis focuses on the initial stages of reshaping, the behavior of which is not strongly tied to the equilibrium shape. Instead, kinetics is controlled by the energy cost of transferring atoms from narrow edge facets or small vertex facets to large (effectively infinite) side facets. This cost increases for wider edge facets or larger vertex facets due to the increased cost of extracting atoms from those facets. These trends can be readily quantified in the low-T regime by exact determination of MEP energetics, $\Delta E(q)$, vs q, thereby allowing the determination of ΔE_{max}. In Fig. 7, the behavior of $\Delta E(q)$ vs q is presented for truncations TR1, TR2, and

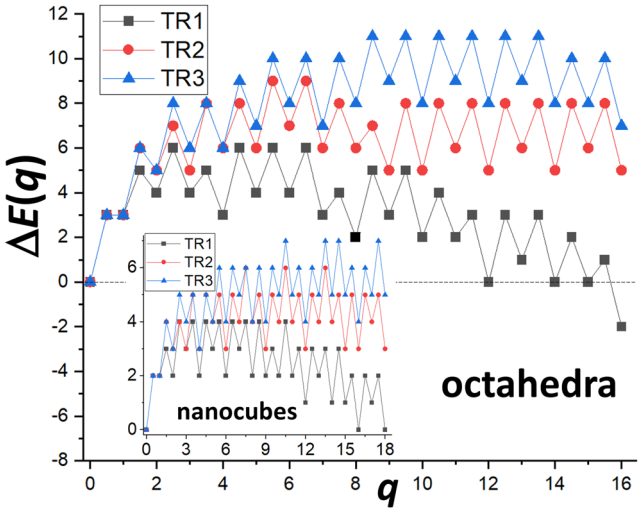

FIG. 7. Energetics, $\Delta E(q)$ vs q, along the minimum energy path for octahedra (and nanocubes in the inset) for truncations TR1, TR2, and TR3. Results for integer q = n give the energy change after n atoms have been removed from vertex (edge) facets for octahedra (nanocubes) and incorporated into a single 2D island on a side facet (e.g., states in the lowest row of Figs. 4 and 6). Values for half-integer q = n + 0.5 correspond to the energy change for states n ⊕ 1, where the (n + 1)st atom has been removed but is not yet incorporated into the 2D island.

TR3 for octahedra (and in the inset for nanocubes). From these plots, it is clear that ΔE_{max} increases systematically with truncation order (as reported above in Sec. IV C 2), and this behavior directly correlates with a corresponding increase in E_{eff}.

V. CONCLUSIONS

Analysis of a realistic stochastic atomistic level model for the reshaping of facetted fcc nanocrystals mediated by nucleation of new layers on side facets has been analyzed. This analysis reveals a fundamental breakdown of the classical free energy picture in CNT for the determination of the effective activation barrier and rate for reshaping. Precise values of the effective barrier obtained from KMC simulation are generally significantly higher than those determined from the free energy barriers for nucleation of 2D islands on side facets. The latter is extracted from constrained equilibrium Monte Carlo simulations of the model which determine the free energy profile during reshaping. Insight into the failure of the free energy-based picture is provided by analysis of reshaping based upon master equations for the model just focusing on the most important nanocrystal configurations or states. This analysis reveals that for these low-barrier reshaping processes, the system is not locally equilibrated before crossing the barrier, as assumed in a free energy-based analysis. This feature results in a smaller entropic reduction to the reshaping barrier than predicted by the CNT analysis.

SUPPLEMENTARY MATERIAL

See the supplementary material for more details on: reshaping of elongated facetted fcc NCs; initial nanocube truncations; KMC results for τ_{eq}; MC simulation of $F(q)$ vs q; analytic assessment of $F(q)$ for small q; characterization of the MEP; configurational degeneracies and rates in master equations for octahedra; and master equations for nanocubes.

ACKNOWLEDGMENTS

This work was supported by the U.S. Department of Energy, Office of Science, Basic Energy Sciences, Division of Chemical Sciences, Geosciences, and Biological Sciences, and was performed in the Computational and Theoretical Chemistry (CTC) project at Ames National Laboratory, which is operated by Iowa State University under Contract No. DE-AC02-07CH11358.

AUTHOR DECLARATIONS

Conflict of Interest

The authors have no conflicts to disclose.

Author Contributions

King C. Lai: Data curation (lead); Formal analysis (equal); Methodology (equal); Software (lead); Validation (equal). **Da-Jiang Liu**: Formal analysis (lead); Investigation (equal). **James W. Evans**: Conceptualization (lead); Formal analysis (equal); Funding acquisition (lead); Investigation (equal); Methodology (equal); Project administration (lead); Supervision (equal); Writing – original draft (lead); Writing – review & editing (lead).

DATA AVAILABILITY

The data that support the findings of this study are available within the article and its supplementary material.

REFERENCES

[1] C. Herring, "Surface tension as a motivation for sintering," in *The Physics of Powder Metallurgy*, edited by W. E. Kingston (McGraw-Hill, New York, 1951), pp. 143–179.
[2] W. W. Mullins, J. Appl. Phys. **30**, 77 (1959).
[3] F. A. Nichols and W. W. Mullins, J. Appl. Phys. **36**, 1826 (1965).
[4] N. Combe, P. Jensen, and A. Pimpinelli, Phys. Rev. Lett. **85**, 110 (2000).
[5] T. H. Lim, D. McCarthy, S. C. Hendy, K. J. Stevens, S. A. Brown, and R. D. Tilley, ACS Nano **3**, 3809 (2009).
[6] D. N. McCarthy and S. A. Brown, Phys. Rev. B **80**, 064107 (2009).
[7] K. C. Lai, Y. Han, P. Spurgeon, W. Huang, P. A. Thiel, D.-J. Liu, and J. W. Evans, Chem. Rev. **119**, 6670 (2019).
[8] Y. Xia, Y. Xiong, B. Lim, and S. E. Skrabalak, Angew. Chem., Int. Ed. **48**, 60 (2009).
[9] Y. Shi, Z. Lyu, M. Zhao, R. Chen, Q. N. Nguyen, and Y. Xia, Chem. Rev. **121**, 649 (2021).
[10] F. Baletto, J. Phys.: Condens. Matter **31**, 113001 (2019).
[11] P. N. Plessow, Phys. Chem. Chem. Phys. **22**, 12939 (2020).
[12] C. Herring, J. Appl. Phys. **21**, 301 (1950).
[13] A. Searcy, J. Am. Ceram. Soc. **68**, C267 (1985).
[14] W. W. Mullins and G. S. Rohrer, J. Am. Ceram. Soc. **83**, 214 (2000).
[15] G. S. Rohrer, C. L. Rohrer, and W. W. Mullins, J. Am. Ceram. Soc. **84**, 2099 (2001).

[16]C. R. Stoldt, A. M. Cadilhe, C. J. Jenks, J.-M. Wen, J. W. Evans, and P. A. Thiel, Phys. Rev. Lett. **81**, 2950 (1998).
[17]P. Jensen, N. Combe, H. Larralde, J. L. Barrat, C. Misbah, and A. Pimpinelli, Eur. Phys. J. B **11**, 497 (1999).
[18]N. Combe and H. Larralde, Phys. Rev. B **62**, 16074 (2000).
[19]D.-J. Liu and J. W. Evans, Phys. Rev. B **66**, 165407 (2002).
[20]H. Zhang, M. Jin, Y. Xiong, B. Lim, and Y. Xia, Acc. Chem. Res. **46**, 1783 (2012).
[21]L. Figueroa-Cosme, K. D. Gilroy, T.-H. Yang, M. Vara, J. Park, S. Bao, A. G. M. da Silva, and Y. Xia, Chem. - Eur. J. **24**, 6133 (2018).
[22]C. Sun, Z. Cao, J. Wang, L. Lin, and X. Xie, New J. Chem. **43**, 2567 (2019).
[23]M. Shao, T. Yu, J. H. Odell, M. Jin, and Y. Xia, Chem. Commun. **47**, 6566 (2011).
[24]A. Matsuda and H. Mori, Chem. Phys. Lett. **644**, 255 (2016).
[25]A. Zalineeva, S. Baranton, C. Coutanceau, and G. Jerkiewicz, Sci. Adv. **3**, e1600542 (2017).
[26]G. Chang, M. Oyama, and K. Hirao, Acta Mater. **55**, 3453 (2007).
[27]H. Ding and J. Dong, Appl. Microsc. **46**, 105 (2016).
[28]A. Pekkari, Z. Say, A. Susarrey-Arce, C. Langhammer, H. Härelind, V. Sebastian, and K. Moth-Poulsen, ACS Appl. Mater. Interfaces **11**, 36196 (2019).
[29]X. Liu, Z. Li, K. Wang, L. Zhou, X. Zhao, W. Jiang, Q. Li, and Y. Deng, Nanomaterials **9**, 375 (2019).
[30]H. Song, F. Kim, S. Connor, G. A. Somorjai, and P. Yang, J. Phys. Chem. B **109**, 188 (2005).
[31]C. T. Lee, X. Yang, M. Vara, K. D. Gilroy, and Y. Xia, ChemNanoMat **3**, 879 (2017).
[32]M. Zhao, Z. Chen, Z. Lyu, Z. D. Hood, M. Xie, M. Vara, M. Chi, and Y. Xia, J. Am. Chem. Soc. **141**, 7028 (2019).
[33]A. Loiudice, P. Lobaccaro, E. A. Kamali, T. Thao, B. H. Huang, J. W. Ager, and R. Buonsanti, Angew. Chem., Int. Ed. **55**, 5789 (2016).
[34]S. Zhou, J. Li, K. D. Gilroy, J. Tao, C. Zhu, X. Yang, X. Sun, and Y. Xia, ACS Nano **10**, 9861 (2016).
[35]S. Lee, C.-U. Kim, and T.-W. Kim, Nanosci. Nanotechnol. **20**, 4525 (2020).
[36]M. Zhao, Z. Chen, Y. Shi, Z. D. Hood, Z. Lyu, M. Xie, M. Chi, and Y. Xia, J. Am. Chem. Soc. **143**, 6293 (2021).
[37]M. Vara, L. T. Roling, X. Wang, A. O. Elnabawy, Z. D. Hood, M. Chi, M. Mavrikakis, and Y. Xia, ACS Nano **11**, 4571 (2017).
[38]K. C. Lai and J. W. Evans, Phys. Rev. Mater. **3**, 026001 (2019).
[39]L. T. Roling, L. Li, and F. Abild-Pedersen, J. Phys. Chem. C **121**, 23002 (2017).
[40]X. He, F. Cheng, and Z.-X. Chen, Sci. Rep. **6**, 33128 (2016).
[41]X. Y. Li, B. Zhu, R. Qi, and Y. Gao, Adv. Theory Simul. **2**, 1800127 (2019).
[42]K. A. Fichthorn and M. Scheffler, Phys. Rev. Lett. **84**, 5371 (2000).
[43]J. W. Evans, P. A. Thiel, and M. C. Bartelt, Surf. Sci. Rep. **61**, 1 (2006).
[44]T. Michely and J. Krug, *Islands, Mounds, and Atoms* (Springer, Berlin, 2004).
[45]K. Morgenstern, Phys. Status Solidi B **242**, 773 (2005).
[46]P. A. Thiel, M. Shen, D.-J. Liu, and J. W. Evans, J. Phys. Chem. C **113**, 5047 (2009).
[47]L. Li, P. N. Plessow, M. Rieger, S. Sauer, R. S. Sánchez-Carrera, A. Schaefer, and F. Abild-Pedersen, J. Phys. Chem. C **121**, 4261 (2017).
[48]K. C. Lai, M. Chen, B. Williams, Y. Han, C.-K. Tsung, W. Huang, and J. W. Evans, ACS Nano **14**, 8551 (2020).
[49]Y. Han, C. R. Stoldt, P. A. Thiel, and J. W. Evans, J. Phys. Chem. C **120**, 21617 (2016).
[50]D. Chandler, *Introduction to Modern Statistical Mechanics* (Oxford University Press, Oxford, 1987).
[51]K. C. Lai, M. Chen, J. Yu, Y. Han, W. Huang, and J. W. Evans, ACS Appl. Mater. Interfaces **13**, 51954 (2021).
[52]N. G. van Kampen, *Stochastic Processes in Physics and Chemistry* (North Holland, Amsterdam, 1981).